OPEN ACCESS
IOP Publishing

Letters
Nanotechnology

Nanotechnology **35** (2024) 48LT02 (9pp) https://doi.org/10.1088/1361-6528/ad6a1f

Letter

Analyte-dependent Rabi splitting in solid-state plexcitonic sensors based on plasmonic nanoislands strongly coupled to J-aggregates

John Carlo Garcia, Ethan Alex Wilson, Dipesh Aggarwal, Harshitha Rajashekhar, Damini Vrushabendrakumar and Karthik Shankar*

Department of Electrical and Computer Engineering, University of Alberta, 9211–116 St, Edmonton AB T6G 1H9, Canada

E-mail: kshankar@ualberta.ca

Received 26 May 2024, revised 7 July 2024
Accepted for publication 1 August 2024
Published 12 September 2024

Abstract

A key challenge in the field of plexcitonic quantum devices is the fabrication of solid-state, device-friendly plexcitonic nanostructures using inexpensive and scalable techniques. Lithography-free, bottom-up nanofabrication methods have remained relatively unexplored within the context of plexcitonic coupling. In this work, a plexcitonic system consisting of thermally dewetted plasmonic gold nanoislands (AuNI) coated with a thin film of J-aggregates was investigated. Control over nanoisland size and morphology allowed for a range of plasmon resonances with variable detuning from the exciton. The extinction spectra of the hybrid AuNI/J-aggregate films display clear splitting into upper and lower hybrid resonances, while the dispersion curve shows anti-crossing behavior with an estimated Rabi splitting of 180 eV at zero detuning. As a proof of concept for quantum sensing, the AuNI/J-aggregate hybrid was demonstrated to behave as a plexcitonic sensor for hydrochloric acid vapor analyte. This work highlights the possibility of using thermally dewetted nanoparticles as a platform for high-quality, tunable, cost-effective, and scalable plexcitonic nanostructures for sensing devices and beyond.

Supplementary material for this article is available online

Keywords: plexcitons, plasmons, excitons, J-aggregates, strong coupling, Rabi-splitting, thermal dewetting

* Author to whom any correspondence should be addressed.

1. Introduction

In recent years, strong coupling phenomena have received significant interest in the areas of photonics, quantum physics, and materials science. Not only do they provide an intriguing opportunity to study exotic light-matter interactions, but they also open up interesting possibilities in fields of quantum information [1], lasers [2], and biochemical sensing [3]. In semiconductor-based systems, strong coupling is typically observed when bound electron-hole pairs (i.e. excitons) strongly interact with cavity modes such as optical mirrors, waveguides, and photonic crystals (cavity quantum electrodynamics [2]). Of particular interest are plasmonic resonators coupled to excitons through plasmon-exciton polaritons to form quasiparticles called 'plexcitons', which receive special attention for enabling room temperature investigation of strong coupling [4]. Strong plexcitonic coupling results in emergent optoelectronic properties distinct from the uncoupled plasmon or exciton. When the plasmon and exciton resonances are closely matched, new hybridized energy states are formed, which manifest spectroscopically as two resonance peaks separated by a transparency dip. The energetic separation between the upper and lower resonances is known as the Rabi splitting (Ω), which is a measure of coupling strength. Whether a system falls in the weak or strong coupling regime depends on a multitude of factors, including detuning between the plasmon and exciton resonances, oscillator strength [5], and plasmon damping [6, 7].

Initial plexcitonic systems focused on excitonic semiconductors coupled to propagating surface plasmon polaritons in planar metallic films [8]. With these rudimentary systems, large values of Rabi splitting can be achieved, however their simple geometry and low tunability limits their practicality. On the other hand, metallic nanoparticles exhibiting localized surface plasmons (LSPs) are extremely versatile as the LSP resonance (LSPR) can be controlled by the nanoparticle's size, shape, composition, and dielectric environment. This flexibility allows for the coupling strength to be conveniently tuned from weak to strong in a given plexcitonic system. As such, many types of metal nanostructure geometries have been used to investigate plasmon-exciton coupling including nanorods [9], nanoprisms [10], nanostars [11], nanorings [12], core-shell nanoparticles [13], and nanoarrays [14]. Among the most widely used excitonic materials coupled to LSPs are J-aggregates—supramolecular assemblies of dye molecules self-organized in a head-to-tail arrangement [15]. This configuration results in the coherent oscillation of transition dipole moments in the constituent molecules, generating an excitonic system with a remarkably large oscillator strength [16]. Spectroscopically, this molecular organization gives rise to a red-shifted absorption feature with an exceptionally narrow linewidth, known as the J-band.

Harnessing strongly coupled plexcitons opens up exciting possibilities for future real-world device applications. Interacting plexcitons have been shown to generate a giant optical nonlinearity and ultrafast optical absorption, enabling energy-efficient all-optical switching and information processing [17]. Likewise, nonlinear quantum plexcitonic systems wherein two or more emitters couple to a single plasmonic nanocavity have been proposed as reconfigurable single photon sources [18]. Plexcitonic systems can be used to extend the spectroscopic molecular ruler effect [19] associated with Förster-type resonance energy transfer to longer distances [7]. The strong coupling of a highly confined plasmonic field to molecular electronic transitions has been proposed as a means to dramatically enhance the rate of spin-forbidden singlet-to-triplet transitions [20] and to generate superradiance [21]. In a molecular plexcitonic system, the change in the refractive index accompanying a molecular spin transition generates a change in the spectral position of the plasmon resonance, thus enabling active plasmonics [22, 23]. Kongsuwan *et al* found that placing a quantum emitter-linked antibody-antigen complex in a nanoplasmonic cavity facilitated strong plexcitonic coupling along with the appearance of signature Rabi splitting at room temperature, which in turn enabled a 15-fold enhancement in sensitivity for an immunoassay compared to classical label-free biosensors based on a binding-induced shift in the plasmon resonance [24].

Many advancements have been made towards the fundamental understanding of plexcitonic coupling between J-aggregates and LSPs; however, less attention has been directed towards developing plexcitonic platforms that are compatible with practical applications. The overwhelming majority of studied plexcitonic systems exist in colloidal form, which are challenging to implement into real-world devices, where solid-state thin films are preferred. While plexcitonic thin films can be inexpensively formed by direct solution casting of J-aggregate/nanoparticle colloids [25], this technique lacks reproducibility and control, as nanoparticle agglomeration and capillary flow can lead to inconsistent and non-uniform films [26]. High quality solid-state plexcitonic films can be created by coating J-aggregates onto lithographically fabricated plasmonic nanostructures such as nanohole [27, 28] or nanodisk arrays [14]. Typically, direct write methods such as electron beam lithography (EBL) and focused ion beam (FIB) milling are employed to achieve plasmonic nanostructures with high periodicity and dimensional accuracy, enabling precise control over the resonance linewidth and damping. However, these methods tend to be expensive, time consuming, and low-throughput, which limits their viability for commercial use. Other top–down fabrication methods, such as nanoimprinting lithography [29], have been investigated as lower cost alternatives, but the prefabricated stamp limits the tunability of the final nanostructure [30]. In order to bring practical plexcitonic devices closer to reality, there is a need for simple, cost-effective, and scalable techniques that allows for the fabrication of tunable, reproducible, and device-friendly plexcitonic nanostructures [31].

Bottom-up approaches to fabricate solid-state plasmonic nanostructures have been seldom explored in the field of plexcitonics. Wurtz *et al* demonstrated a tunable plexcitonic nanostructure consisting of electrochemically grown gold nanorod arrays coated with a thin film of J-aggregates [9]. The nanorod

diameter, length, and spacing were tuned to easily modulate the resonance frequency and coupling strength, demonstrating the possibility of tunable plexcitonic structures using simple and scalable techniques. A well-established bottom-up nanofabrication method for creating plasmonic nanoparticles is solid-state thermal dewetting [32]. Thermal dewetting is a cost-effective, reproducible, and high-throughput means of fabricating plasmonic nanostructures on a substrate. This technique consists of vacuum deposition followed by thermal annealing, which allows for flexibility in modulating the LSPR frequency via simple modifications to processing parameters [33, 34]. While thermally dewetted nanoparticles have been implemented in applications such as photovoltaics [35], organic light emitting diodes [36], and photocatalysis [33], it remains unexplored as a platform for strong plasmon-exciton coupling. Despite the potential to achieve relatively high Q-factors using this technique [37], thermal dewetted nanoparticles tend to exhibit higher degrees of polydispersity, resulting in generally broader resonances compared to plasmonic nanostructures fabricated using EBL or FIB milling. As such, a longstanding question in the field relates to whether true quantum entanglement is achievable in a system with large homogeneous and inhomogeneous broadening.

In this work, strong plasmon-exciton coupling was investigated in a hybrid nanostructure consisting of thermally dewetted gold nanoislands (AuNI) coated with a thin film of J-aggregates. We employ a lithography-free process consisting of simple vacuum deposition, thermal annealing, and spin coating. By modulating the deposition time, we control nanoisland size and plasmon resonances, allowing for the study of coupling behaviour near and away from the resonant conditions. We show that the AuNI/J-aggregate hybrid conclusively satisfies the strong coupling criterion, demonstrating clear anti-crossing behavior and a Rabi splitting of 180 meV. As a proof of concept for device-based applications, the AuNI/J-aggregate hybrid was tested as an optical sensor for hydrochloric acid vapor. This work showcases the potential of using thermally dewetted nanoparticles as a cost-effective and mass production compatible platform for creating solid-state plexcitonic devices.

2. Materials & methods

2.1. Materials

1,1′-Diethyl-2,2′-cyanine iodide (97%) was purchased from TCI Chemicals. Sodium chloride was purchased from Fisher Scientific. Fluorine-doped tin oxide (FTO) coated glass substrates (TEC 8) were obtained from Hartford Tec Glass Company. Hydrochloric acid (37%) was obtained from Sigma Aldrich.

2.2. Formation of J-aggregate, Au nanoislands, and hybrid plexcitonic structure

The J-aggregate was formed by adding 1 mg of 1,1′-diethyl-2,2′-cyanine iodide (pseudoisocyanine iodide or PIC) and 42 mg of sodium chloride to 4 ml of deionized water based on previously reported methods [38]. The solution was heated to 80 °C using a hot bath and kept for 40 min. The solution was room cooled and aged in the dark for 5 h before use. Plasmonic gold nanoislands (AuNI) were formed using a solid state thermal dewetting process consisting of deposition followed by annealing. Prior to deposition, the FTO substrates were cleaned via ultrasonication in isopropyl alcohol, methanol, and deionized water. Gold deposition was performed using a Kurt J Lesker CMS-18 DC magnetron sputtering system using an average deposition rate of 7.6 nm min^{-1}. To achieve a range of plasmon resonances, the sputtering time was varied from 20 to 70 s while deposition pressure was fixed at 15 mTorr. Subsequently, the as-deposited films were annealed together at 500 °C in an open-air tube furnace following a 4 hour ramp/4 hour dwell heating profile followed by air-cooling to room temperature. The slow ramp up rate and air-cooling inside the furnace was necessary to prevent fracture of the substrate due to thermal shock. The plexcitonic hybrid nanostructure was formed via spin coating the J-aggregates onto the Au nanoislands. A small amount of J-aggregate solution (30 μl) was deposited onto the nanoislands followed by a 60 s rest period to promote adhesion of the J-aggregate to the gold nanoisland surface. Spin coating was performed at 2000 RPM for 60 s to form the final plexcitonic hybrid.

2.3. Characterization of J-aggregate, Au-nanoislands and hybrid structure

The extinction spectra of the J-aggregates, Au nanoislands, and hybrid nanostructures were collected using a UV-VIS spectrophotometer (Perkin–Elmer Lambda 900 UV/VIS/NIR). Special care was taken to ensure consistent beam alignment during scanning of the Au nanoislands prior to and after coating with J-aggregates to minimize error due to beam positioning. The baseline spectrum for the FTO substrate was subtracted from plotted spectra. Scanning electron microscopy (Zeiss Sigma FESEM) was performed to study the morphology of the plasmonic nanoislands and hybrid. Nanoisland size distributions were extracted from SEM images via ImageJ. To account for shape polydispersity, nanoisland size is based on the diameter of an equivalent circle based on the nanoisland area. Particles under 14 nm in diameter were omitted from the image analysis to prevent erroneous measurements due to the resolution limits of the SEM images. The resulting size distributions were weighted based on area fraction. High resolution transmission electron microscopy (JEOL JEM-ARM200CF HRTEM) was performed on a FIB-prepared lamella of gold nanoislands on FTO. Grazing incidence x-ray diffraction (Rigaku Ultima IV, Cu K-α source) was performed to validate the crystallographic d-spacing as obtained from HRTEM.

2.4. Gas sensing and long-term stability experiments

Gas sensing experiments were performed using a test chamber consisting of a sealed container with a moat configuration. The

experimental setup and process flowchart for the gas sensing experiments can be found in supporting information, figure S1. The container was filled with 10 ml hydrochloric acid solutions of varying concentrations (10 M, 5 M, and 2.5 M). A platform to elevate the sample above the solution was placed in the center of the chamber, forming a moat. The chamber was sealed using a lid with a 1.5 mm pinhole to prevent excessive pressure build-up. The exterior of the chamber was wrapped with aluminum foil to ensure dark conditions and mitigate possible photobleaching caused by stray ambient light. Prior to loading the sample, the chamber was pre-heated to 80 °C to produce an adequate amount of vapor flux. After 5 min of preheating, the sample was placed in the chamber and exposed for a predetermined time interval. Following each time interval, UV-VIS spectroscopy was performed to observe the change in the extinction spectra. After the acquisition of spectra, the sample was then placed in the chamber again to be exposed for another pre-determined amount of time until a total accumulated exposure time was reached. The long-term stability of the AuNI/J-aggregate was tested by storing the plexcitonic hybrid sample in dark and light ambient conditions over extended periods of time and periodically collecting the UV-VIS spectrum to ascertain changes in coupling strength.

3. Results & discussion

3.1. Overview of AuNI/J-aggregate plexcitonic hybrid

The fabrication process of the hybrid plexcitonic nanostructure via solid state thermal dewetting is summarized in figure 1(a). DC magnetron sputtering was used to deposit gold onto FTO substrates (figure 1(b)), resulting in a thin Au film (figure 1(c)). The as-deposited Au film was annealed in a tube furnace, resulting in plasmonic gold nanoislands (figure 1(d)). Deposition and annealing parameters are based on previously reported conditions known to produce gold nanoislands with LSPRs in the range of the expected J-band (i.e. ∼580 nm) [39]. A critical factor for reproducibility is minimizing region-to-region variability in film thickness and coverage. This was achieved by using a relatively high deposition pressure (i.e. 15 mTorr) to provide a more diffuse deposition flux, resulting in improved film uniformity. Furthermore, a tubular furnace was used for annealing due to its uniform heating profile along the length of the tube. As a result, reproducible resonance characteristics were obtained across a given sample and between multiple samples (see supporting information, figure S2 and table S1). HRTEM images of the dewetted Au nanoislands clearly show the (111) crystallographic planes of the Au nanoislands, while the corresponding lattice spacing of $d = 0.24$ nm matches the 2-theta value of 37.4° observed using XRD (figure S3).

Pseudoisocyanine iodide (PIC) J-aggregates were used as the excitonic material and were spin coated onto the nanoislands to form the plexcitonic nanostructure (figure 1(e)). Fluorine doped tin-oxide (TEC8) was specifically selected as a substrate material due to its inherent surface roughness as well as optical transparency. Since the J-aggregate solution has poor wettability on smooth glass, the increased surface roughness of FTO is expected to enhance lyophilicity with the J-aggregate solution during spin-casting, allowing for a more well-adhered film that maximizes the intimacy between plasmon and exciton. Indeed, figure 1(e) shows close proximity between the J-aggregate film and plasmon, with a J-aggregate film thickness of approximately 150–200 nm (figure S4). It is worth pointing out that the spin casting process did not alter the arrangement of nanoislands, owing to the robustness of the thermally dewetted nanostructure. Interestingly, the resultant J-aggregate film does not consist of a uniform and conformal layer, leaving some areas of exposed nanoislands. Despite this, the ensemble still displayed strong coupling behavior, as will be discussed later.

3.2. Investigation of uncoupled plasmon and exciton

To investigate plasmon-exciton coupling across a wide range of plasmon resonances, the size of the nanoislands was tuned by varying the deposition time. Figure 2 shows the morphology and normalized extinction spectra of five representative Au nanoisland samples with plasmon frequencies ranging between 1.97 and 2.15 eV. The samples (N1 to N5) are ordered sequentially from shortest to longest deposition time. Compared to film thickness, deposition time is a more meaningful metric to measure as film thickness is not well-defined at such scales. At shorter deposition times, Volmer–Weber island growth dominates, resulting in largely discontinuous films without a well-defined thickness (figure S5). As deposition time increases, the films become increasingly continuous, and thickness becomes more well-defined. Table 1 summarizes characteristics related to the nanoisland size and plasmon resonance of the five representative Au nanoisland samples. Additional details regarding size distributions and plasmon linewidth calculations can be found in the supporting information.

Scanning electron microscopy (figure 2(a)) reveals a gradual rise in overall nanoisland size as deposition time increases, increasing from a mean diameter of 19–124 nm. The increase in size is accompanied by a redshift in the LSPR towards longer wavelengths i.e. from 578 to 630 nm (figure 2(b)), which is expected behaviour. As average size and LSPR wavelength increase, a concomitant broadening of the resonance linewidth is observed, caused by growing contributions of radiative damping and inhomogeneous broadening. As radiative damping is proportional to the nanoparticle volume, homogeneous broadening is expected as particle size increases. Likewise, as nanoisland diameter grows, a clear increase in size and shape polydispersity can be observed (figures S6 and S7), significantly contributing to inhomogeneous broadening. Smaller nanoislands exhibit a roughly circular profile with little variation in size and shape. At intermediate sizes, the shape becomes elongated and gives rise to irregular geometries due to the coalescence of adjacent islands. At large sizes, the nanoislands develop a flat-top structure with faceted edges as it tends towards its equilibrium shape. This

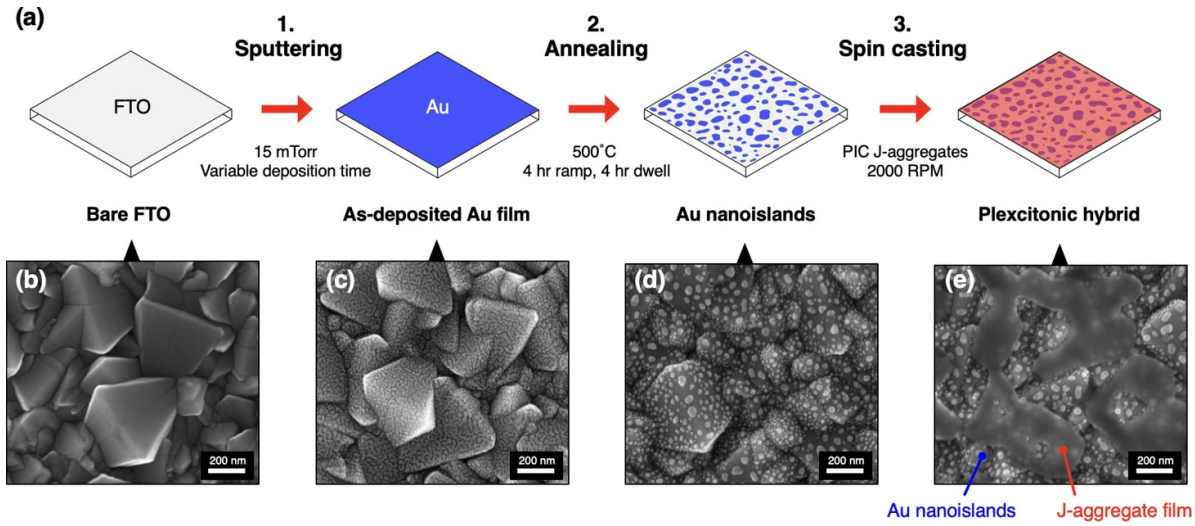

Figure 1. (a) Fabrication process of AuNI/J-aggregate hybrid plexcitonic nanostructure with SEM images of (b) bare FTO, (c) sputtered Au film, (d) thermally dewetted Au nanoislands, and (e) AuNI/J-aggregate plexcitonic hybrid.

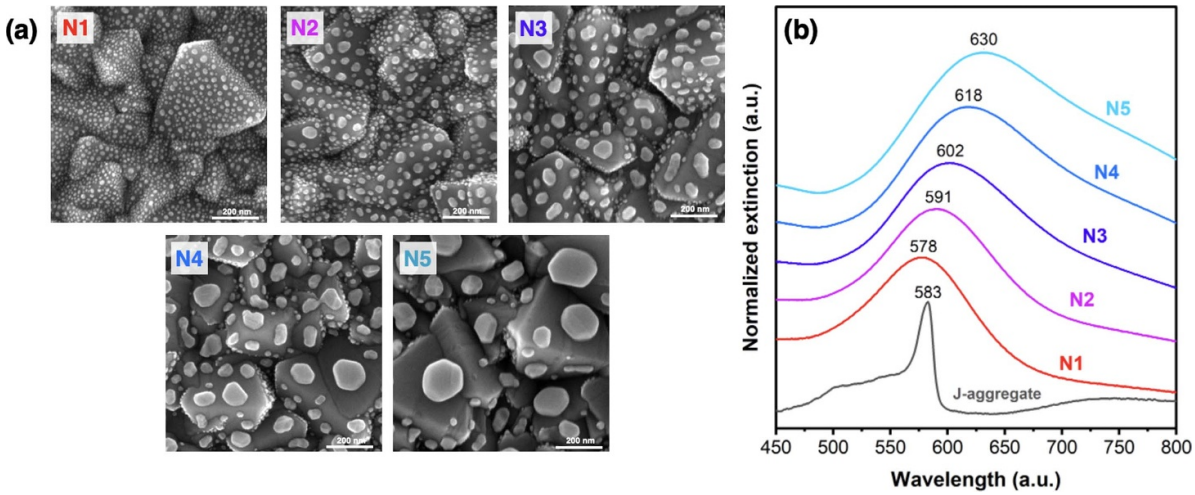

Figure 2. (a) Scanning electron micrographs of Au nanoislands of different average sizes (b) normalized extinction spectra of Au nanoislands and J-aggregate film.

Table 1. Size and resonance peak parameters of Au nanoislands.

Sample	Mean diameter (nm)	Standard deviation (nm)	LSPR, λ_{pl} (nm)	Plasmon energy, E_{pl} (eV)	FWHM, Γ_{pl} (meV)	Detuning, δ (meV)
N1	19	4	578	2.15	320	+18
N2	31	11	591	2.10	335	−29
N3	50	20	602	2.06	391	−67
N4	75	28	618	2.01	441	−121
N5	124	45	630	1.97	517	−159

flat-top geometry is clearly visible in cross-sectional TEM photos of the nanoislands (figure S3) and is consistent with typical thermally dewetted nanostructures [40]. It is worth noting that the inherent three-dimensionality of the FTO grains significantly contributes to size polydispersity. The flat surfaces of FTO grains orthogonal to the sputtering target are likely to receive a larger deposition flux than surfaces pointed away, resulting in thicker and more continuous films on flat surfaces versus tilted or near-vertical surfaces (see supporting information figure S5). The direct consequence of this is that nanoislands formed on flat surfaces tend to be larger in size, contributing to the overall polydispersity and inhomogeneous broadening as initial deposition time increases. The extinction spectra of the uncoupled J-aggregate thin film can also be seen in figure 2(b). The J-band is centered at 583 nm ($E_{ex} = 2.13$ eV) with an exciton linewidth of $\Gamma_{ex} = 70.4$ meV.

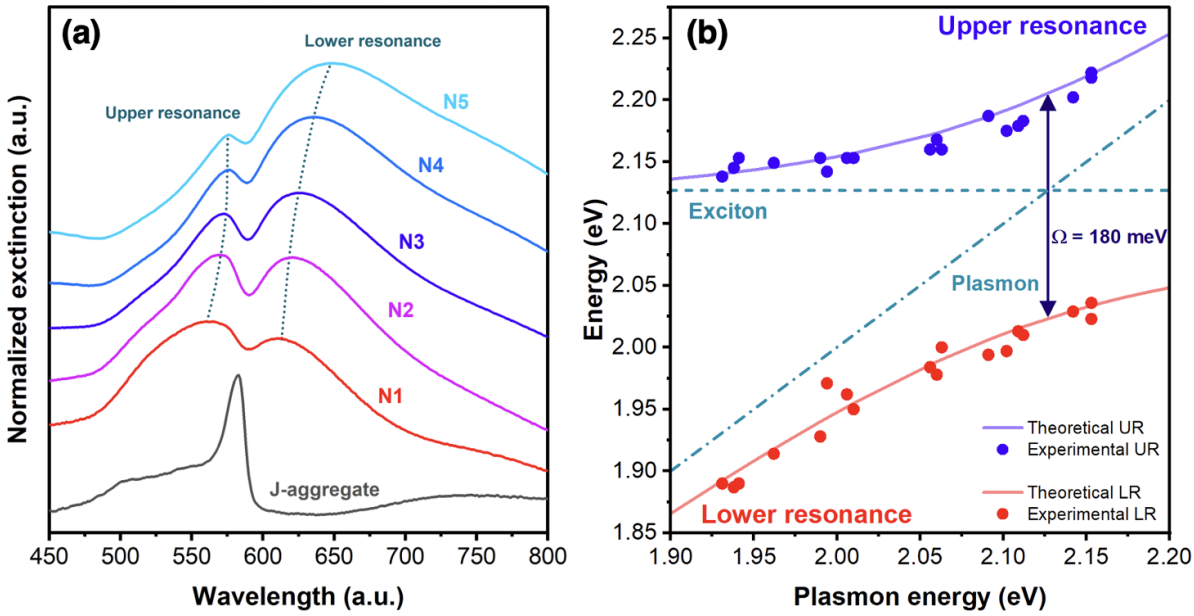

Figure 3. (a) Normalized extinction spectra of AuNI/J-aggregate plexcitonic hybrid (b) dispersion curve of AuNI/J-aggregate hybrid with theoretical and experimental resonances.

The broad tail-like absorption occurring sub-560 nm corresponds to weak contributions from the monomer (545 nm) and H-aggregate (504 nm) bands [38].

3.3. Investigation of plasmon-exciton coupling in AuNI/J-aggregate hybrid

The extinction spectra of the AuNI/J-aggregate plexcitonic hybrid is shown in figure 3(a). Coating of J-aggregates onto the Au nanoislands resulted in the splitting of the optical spectra and emergence of two hybrid energy peaks in all samples tested. The newly formed resonances are separated by a transparency dip centered near the J-band frequency. Relative to the transparency dip, the blue-shifted and red-shifted peaks correspond to the upper and lower plexcitonic resonances, respectively. It can be seen that the spectral profiles of the upper resonance (UR) and lower resonance (LR) are strongly dependent on the detuning (δ) between the plasmon and exciton resonances (i.e. $\delta = E_{\mathrm{pl}} - E_{\mathrm{ex}}$). Sample N1, which represents the closest to resonance conditions ($\delta = +18$ meV), exhibits an asymmetrical profile biased towards the UR. As the plasmon is negatively detuned from the exciton resonance (i.e. increasing LSPR wavelength), the profile becomes gradually skewed towards the LR. As the detuning becomes very large, the LR is dominant while the UR converges towards the exciton resonance.

An important characteristic of strongly coupled hybrid systems is the avoided crossing or anti-crossing of the dispersion curves. This can be modeled classically by treating the system as two coupled harmonic oscillators [41]. Figure 3(b) shows the theoretical and experimental dispersion for the AuNI/J-aggregate hybrid system. The expected behavior of the system if uncoupled is represented by the dashed exciton and plasmon lines. The theoretical energies of the upper (E_{UR}) and lower (E_{LR}) plexcitonic resonances when strongly coupled is described by the following relationship [41]:

$$E_{\mathrm{UR/LR}} = \frac{1}{2}\left(E_{\mathrm{pl}} + E_{\mathrm{ex}}\right) \pm \sqrt{g^2 + \frac{\delta^2}{4}} \qquad (1)$$

where E_{pl} and E_{ex} are the plasmonic and excitonic resonances (in eV), respectively. The coupling constant g relates to the energy separation between the upper and lower resonances where Rabi splitting Ω is related to the coupling constant by $\Omega = 2\,g$. The value δ corresponds to the detuning between plasmon and exciton energies. As seen in figure 3(b), the experimental upper and lower resonances closely adhere to the calculated theoretical values, strongly suggesting anti-crossing behavior in the AuNI/J-aggregate system. The Rabi splitting can be estimated by measuring the energy difference between the upper and lower resonances at zero detuning. Using fitted theoretical resonance curves to our experimental data, the Rabi splitting is estimated to be 180 meV. Comparing this value to similar solid-state plexcitonic systems, it can be seen that our system outperforms films cast from colloidal solutions [25] as well as other bottom–up approaches [9]. In general, plexcitonic systems based on lithographically-formed metasurfaces tend to obtain higher values of Rabi splitting [14, 27, 28], which is unsurprising due to better control over distributions in size, shape, and spacing. Compared to solution phase plexcitonic systems, the obtained Rabi splitting is comparable to many Au/PIC-based J-aggregate colloidal plexcitonic systems [42, 43]. However, it is worth noting that discrete nanoparticles with high aspect ratio features (e.g. nanorods, nanostars, nanoprisms) allow the achievement of larger Rabi splitting values [43–46].

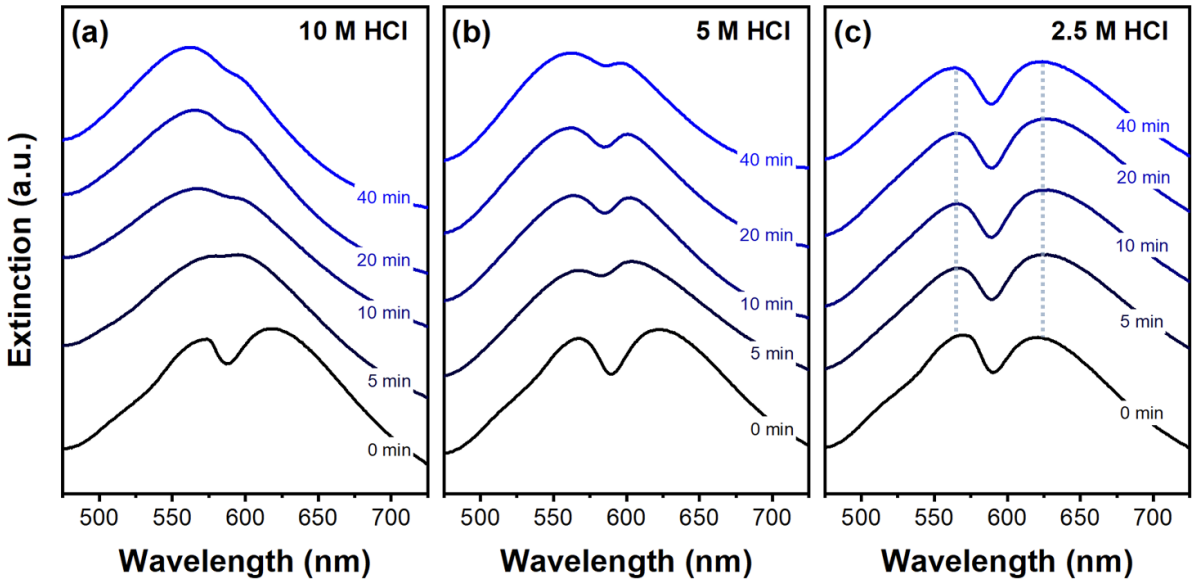

Figure 4. Optical gas sensing experiments using AuNI/J-aggregate plexcitonic hybrid using different concentrations of HCl; (a) 10 M, (b) 5 M, and (c) 2.5 M.

Demonstration of anti-crossing behavior is typically insufficient to definitively prove strong coupling. Whether the system is within the weak or strong coupling regime is dependent on (i) the rate of coherent energy exchange between the plasmon and exciton, and (ii) the rate of damping losses in the system [41]. A system is said to be in the weak coupling regime if the rate of damping exceeds the rate of energy exchange. Conversely, a system is strongly coupled if the rate of energy exchange is larger than the rate of damping. In other words, in a strongly coupled system, the observed Rabi splitting must be large in comparison to the linewidths of the plasmon and exciton and must satisfy the following relation:

$$\Omega_R^2 > \left(\frac{\Gamma_{ex}}{2} - \frac{\Gamma_{pl}}{2}\right)^2. \tag{2}$$

As none of the nanoisland plasmon resonances matched exactly with exciton resonance, nanoisland N1 was used for calculation as it had the smallest detuning ($\delta = -18$ meV). Substituting the corresponding linewidths for plasmon and exciton ($\Gamma_{pl} = 320$ meV and $\Gamma_{ex} = 70.4$ meV), it can be seen that the strong coupling criterion is met if the Rabi splitting is larger than 125 meV. Our observed Rabi splitting of 180 meV more than satisfies this criterion, conclusively placing our AuNI/J-aggregate hybrid in the strong coupling regime.

3.4. Gas sensing experiments

As a proof-of-concept for solid state device applications, the hybrid AuNI/J-aggregate plexcitonic system was used as a platform for optical gas sensing. The concept behind an optical plexcitonic sensor is based on the fact the coupling strength is highly sensitive to perturbations in the plasmon and exciton. Slight changes to the plasmon frequency (i.e. detuning) and exciton oscillator strength are enough to influence the presence and magnitude of Rabi splitting as well as the energies of the hybrid resonances. This operating principle shares similarities to induced transparency sensors [47], however its worth mentioning that many of these platforms are in the weak coupling regime. Only recently has quantum plexcitonic sensing in the strong coupling regime been demonstrated [48]. Vapor phase systems offer a convenient means to perturb either the plasmon, exciton, or their coupling. As organic films are permeable to vapors, analytes are able to reach the J-aggregate and gold nanoisland interface, where coupling occurs. Depending on the analyte, certain chemical reactions can occur resulting in oxidation or etching of the J-aggregate, in turn affecting its oscillator strength. Vapors can also affect plasmons by preferentially binding to either the metal or the J-aggregate and altering the surrounding permittivity. Taking this into consideration, vapor phase systems are an ideal platform for demonstrating a proof-of-concept plexcitonic sensor.

To demonstrate the sensing capabilities of the AuNI/J-aggregate hybrid, the plexcitonic film was exposed to hydrochloric acid (HCl) vapor and the temporal evolution of Rabi splitting was monitored. A schematic of the experimental setup can be seen in figure S1 in the supporting information. Three concentrations (10 M, 5 M and 2.5 M) were selected to demonstrate three regimes of sensing as shown in figure 4. At very high concentrations (figure 4(a)), the Rabi splitting can be seen to disappear completely after 5 min of exposure. This is likely caused by the oxidation of the J-aggregate in response to the corrosive vapor, resulting in a reduction of oscillator strength and loss of coupling. As exposure time increases, the overall profile of the spectrum blue shifts, and what appears to be the upper resonance begins to dominate. Interestingly, the profile does not revert back to the uncoupled LSPR position, and a weak shoulder feature is preserved. At intermediate

concentrations (figure 4(b)), the Rabi splitting is reduced significantly after 5 min, however the upper and lower resonances are still clearly distinguishable. Further exposure results in a slight blue-shifting of the overall profile. At low concentrations (figure 4(c)), Rabi splitting remains unchanged even after 40 min of exposure. Despite this, a slight broadening of the upper and lower resonance can still be observed as exposure time increases. Follow up investigations are needed to elucidate these findings.

The stability and longevity of the AuNI/J-aggregate hybrid appear to be most sensitive to factors that directly influence the J-aggregate oscillator strength, such as the concentration of corrosive vapor or photodegradation. Long term stability experiments were performed to assess the stability of the plexcitonic hybrid in ambient conditions and in the absence of light. Remarkably, it can be seen that the strong coupling remains largely preserved even after 60 d of storage in dark ambient conditions (figure S8(a)). In contrast, storage in ambient lighting conditions results in significant loss of coupling after only three days (figure S8(b)). This is unsurprising due to the well-known photostability issues of organic semiconductors; however, these results highlight the sensitivity of the AuNI/J-aggregate plexcitonic sensor to changes in oscillator strength. Further investigations are needed to understand how selective perturbation of the plasmon frequency influences the plexcitonic coupling of the hybrid nanostructure. Nonetheless, these results highlight the possibility of the AuNI/J-aggregate plexcitonic system as a novel platform for optical sensing.

It is worth noting that a more ideal quantum sensor would consist of a single gold nanoisland in contact with a monolayer of J-aggregates, whose optical sensing characteristics can be observed using near-field scanning optical microscopy. In a single nanoisland, inhomogeneous broadening can be ignored and only intrinsic damping would be considered, resulting in a narrower linewidth and improved coupling. Furthermore, a J-aggregate monolayer would increase sensitivity due to the absence of uncoupled J-aggregates from the bulk film, which may currently act as a protective barrier, reducing sensitivity.

4. Conclusion

In summary, we report a novel platform for tunable, scalable, device-friendly plexcitonic structures consisting of thermally dewetted gold nanoislands coated with a thin film of J-aggregates. The AuNI/J-aggregate hybrid system displayed anti-crossing behavior with an estimated Rabi splitting as large as 180 meV, which is markedly improved from other solid-state configurations based on drop casting and self-assembly. As a proof-of-concept, the plexcitonic hybrid was demonstrated as a Rabi splitting based optical gas sensor using HCl vapor as the analyte, highlighting its potential use in device-based applications. The demonstration of reproducible and tunable solid-state plexcitonic coupling using lithography-free processes represents a remarkable step from an accessibility and commercial standpoint. Not only does this allow for easier integration of plexcitons into real devices, but it also facilitates the development and prototyping of novel plexcitonic devices, paving the way for new opportunities in applying strong coupling phenomena.

Data availability statement

The data cannot be made publicly available upon publication because they contain commercially sensitive information. The data that support the findings of this study are available upon reasonable request from the authors.

Acknowledgments

This research is supported by the National Sciences and Engineering Research Council of Canada (NSERC) and Alberta Innovates.

ORCID iDs

John Carlo Garcia https://orcid.org/0000-0002-5964-5781
Harshitha Rajashekhar https://orcid.org/0000-0002-8019-4970
Karthik Shankar https://orcid.org/0000-0001-7347-3333

References

[1] Blais A, Girvin S M and Oliver W D 2020 Quantum information processing and quantum optics with circuit quantum electrodynamics *Nat. Phys.* **16** 247–56
[2] Yu X, Yuan Y, Xu J, Yong K, Qu J and Song J 2019 Strong coupling in microcavity structures: principle, design, and practical application *Laser Photon. Rev.* **13** 1800219
[3] Kim Y, Barulin A, Kim S, Lee L P and Kim I 2022 Recent advances in quantum nanophotonics: plexcitonic and vibro-polaritonic strong coupling and its biomedical and chemical applications *Nanophotonics* **12** 413–39
[4] Zengin G, Wersäll M, Nilsson S, Antosiewicz T J, Käll M and Shegai T 2014 Realizing strong light-matter interactions between single-nanoparticle plasmons and molecular excitons at ambient conditions *Phys. Rev. Lett.* **114** 157401
[5] Thomas R, Thomas A, Pullanchery S, Joseph L, Somasundaran S M, Swathi R S, Gray S K and Thomas K G 2018 Plexcitons: the role of oscillator strengths and spectral widths in determining strong coupling *ACS Nano* **12** 402–15
[6] Kumar M, Dey J, Verma M S and Chandra M 2020 Nanoscale plasmon–exciton interaction: the role of radiation damping and mode-volume in determining coupling strength *Nanoscale* **12** 11612–8
[7] Manuel A P, Kirkey A, Mahdi N and Shankar K 2019 Plexcitonics—fundamental principles and optoelectronic applications *J. Mater. Chem.* C **7** 1821–53
[8] Bellessa J, Bonnand C, Plenet J C and Mugnier J 2004 Strong coupling between surface plasmons and excitons in an organic semiconductor *Phys. Rev. Lett.* **93** 036404
[9] Wurtz G A, Evans P R, Hendren W, Atkinson R, Dickson W, Pollard R J, Zayats A V, Harrison W and Bower C 2007 Molecular plasmonics with tunable exciton−plasmon coupling strength in J-aggregate hybridized Au nanorod assemblies *Nano Lett.* **7** 1297–303
[10] Balci S 2013 Ultrastrong plasmon–exciton coupling in metal nanoprisms with J-aggregates *Opt. Lett.* **38** 4498
[11] Melnikau D, Savateeva D, Susha A, Rogach A L and Rakovich Y P 2013 Strong plasmon-exciton coupling in a

hybrid system of gold nanostars and J-aggregates *Nanoscale Res. Lett.* **8** 134
[12] Li N, Han Z, Huang Y, Liang K, Wang X, Wu F, Qi X, Shang Y, Yu L and Ding B 2020 Strong plasmon–exciton coupling in bimetallic nanorings and nanocuboids *J. Mater. Chem.* C **8** 7672–8
[13] Fofang N T, Park T-H, Neumann O, Mirin N A, Nordlander P and Halas N J 2008 Plexcitonic nanoparticles: plasmon−exciton coupling in nanoshell−J-aggregate complexes *Nano Lett.* **8** 3481–7
[14] Bellessa J *et al* 2009 Giant Rabi splitting between localized mixed plasmon-exciton states in a two-dimensional array of nanosize metallic disks in an organic semiconductor *Phys. Rev.* B **80** 033303
[15] Würthner F, Kaiser T E and Saha-Möller C R 2011 J-aggregates: from serendipitous discovery to supramolecular engineering of functional dye materials *Angew. Chem., Int. Ed.* **50** 3376–410
[16] Bricks J L, Slominskii Y L, Panas I D and Demchenko A P 2017 Fluorescent J-aggregates of cyanine dyes: basic research and applications review *Methods Appl. Fluoresc.* **6** 012001
[17] Tang Y, Zhang Y, Liu Q, Wei K, Cheng X, Shi L and Jiang T 2022 Interacting plexcitons for designed ultrafast optical nonlinearity in a monolayer semiconductor *Light Sci. Appl.* **11** 94
[18] You J-B *et al* 2020 Reconfigurable photon sources based on quantum plexcitonic systems *Nano Lett.* **20** 4645–52
[19] Sobakinskaya E, Schmidt Am Busch M and Renger T 2018 Theory of FRET "spectroscopic ruler" for short distances: application to polyproline *J. Phys. Chem.* B **122** 54–67
[20] Duan S, Rinkevicius Z, Tian G and Luo Y 2019 Optomagnetic effect induced by magnetized nanocavity plasmon *J. Am. Chem. Soc.* **141** 13795–8
[21] Wang S and Hsu L-Y 2023 Exploring superradiance effects of molecular emitters coupled with cavity photons and plasmon polaritons: a perspective from macroscopic quantum electrodynamics *J. Phys. Chem.* C **127** 12904–12
[22] Gural'skiy I A, Quintero C M, Abdul-Kader K, Lopes M, Bartual-Murgui C, Salmon L, Zhao P, Molnár G, Astruc D and Bousseksou A 2012 Detection of molecular spin-state changes in ultrathin films by photonic methods *J. Nanophoton.* **6** 063517–1–063517–13
[23] Abdul-Kader K *et al* 2013 Synergistic switching of plasmonic resonances and molecular spin states *Nanoscale* **5** 5288–93
[24] Kongsuwan N, Xiong X, Bai P, You J-B, Png C E, Wu L and Hess O 2019 Quantum plasmonic immunoassay sensing *Nano Lett.* **19** 5853–61
[25] Song T, Chen Z, Zhang W, Lin L, Bao Y, Wu L and Zhou Z-K 2019 Compounding plasmon–exciton strong coupling system with gold nanofilm to boost Rabi splitting *Nanomaterials* **9** 564
[26] Kumar A K S, Zhang Y, Li D and Compton R G 2020 A mini-review: how reliable is the drop casting technique? *Electrochem. Commun.* **121** 106867
[27] Dintinger J, Klein S, Bustos F, Barnes W L and Ebbesen T W 2004 Strong coupling between surface plasmon-polaritons and organic molecules in subwavelength hole arrays *Phys. Rev.* B **71** 035424
[28] Wang H *et al* 2016 The role of Rabi splitting tuning in the dynamics of strongly coupled J-aggregates and surface plasmon polaritons in nanohole arrays *Nanoscale* **8** 13445–53
[29] Chantharasupawong P, Tetard L and Thomas J 2014 Coupling enhancement and giant Rabi-splitting in large arrays of tunable plexcitonic substrates *J. Phys. Chem.* C **118** 23954–62
[30] Yang K, Yao X, Liu B and Ren B 2021 Metallic plasmonic array structures: principles, fabrications, properties, and applications *Adv. Mater.* **33** e2007988
[31] Chen Y and Sun M 2023 Plexcitonics: plasmon–exciton coupling for enhancing spectroscopy, optical chirality, and nonlinearity *Nanoscale* **15** 11834–51
[32] Gentili D, Foschi G, Valle F, Cavallini M and Biscarini F 2012 Applications of dewetting in micro and nanotechnology *Chem. Soc. Rev.* **41** 4430–43
[33] Manuel A P, Barya P, Riddell S, Zeng S, Alam K M and Shankar K 2020 Plasmonic photocatalysis and SERS sensing using ellipsometrically modeled Ag nanoisland substrates *Nanotechnology* **31** 365301
[34] Thompson C V 2012 Solid-state dewetting of thin films *Annu. Rev. Mater. Res.* **42** 399–434
[35] Fleetham T, Choi J-Y, Choi H W, Alford T, Jeong D S, Lee T S, Lee W S, Lee K-S, Li J and Kim I 2015 Photocurrent enhancements of organic solar cells by altering dewetting of plasmonic Ag nanoparticles *Sci. Rep.* **5** 14250
[36] Shin J-W *et al* 2014 Random nano-structures as light extraction functionals for organic light-emitting diode applications *Org. Electron.* **15** 196–202
[37] Sun H, Yu M, Wang G, Sun X and Lian J 2012 Temperature-dependent morphology evolution and surface plasmon absorption of ultrathin gold island films *J. Phys. Chem.* C **116** 9000–8
[38] Struganova I A, Hazell M, Gaitor J, McNally-Carr D and Zivanovic S 2003 Influence of inorganic salts and bases on the J-band in the absorption spectra of water solutions of 1,1'-diethyl-2,2'-cyanine iodide *J. Phys. Chem.* A **107** 2650–6
[39] Manuel A P *et al* 2022 Hot carrier photocatalysis using bimetallic Au@Pt hemispherical core–shell nanoislands *J. Mater. Sci., Mater. Electron.* **33** 18134–55
[40] Preston A S, Hughes R A, Demille T B, Davila V M R and Neretina S 2019 Dewetted nanostructures of gold, silver, copper, and palladium with enhanced faceting *Acta Mater.* **165** 15–25
[41] Törmä P and Barnes W L 2015 Strong coupling between surface plasmon polaritons and emitters: a review *Rep. Prog. Phys.* **78** 013901
[42] Liu R, Zhou Z-K, Yu Y-C, Zhang T, Wang H, Liu G, Wei Y, Chen H and Wang X-H 2017 Strong light-matter interactions in single open plasmonic nanocavities at the quantum optics limit *Phys. Rev. Lett.* **118** 237401
[43] Das K, Dey J, Verma M S, Kumar M and Chandra M 2020 Probing the role of oscillator strength and charge of exciton forming molecular J-aggregates in controlling nanoscale plasmon–exciton interactions *Phys. Chem. Chem. Phys.* **22** 20499–506
[44] Melnikau D, Samokhvalov P, Sánchez-Iglesias A, Grzelczak M, Nabiev I and Rakovich Y P 2022 Strong coupling effects in a plexciton system of gold nanostars and J-aggregates *J. Lumin.* **242** 118557
[45] Melnikau D, Esteban R, Savateeva D, Sańchez-Iglesias A, Grzelczak M, Schmidt M K, Liz-Marzán L M, Aizpurua J and Rakovich Y P 2016 Rabi splitting in photoluminescence spectra of hybrid systems of gold nanorods and J-aggregates *J. Phys. Chem. Lett.* **7** 354–62
[46] Das K, Hazra B and Chandra M 2017 Exploring the coherent interaction in a hybrid system of hollow gold nanoprisms and cyanine dye J-aggregates: role of plasmon-hybridization mediated local electric-field enhancement *Phys. Chem. Chem. Phys.* **19** 27997–8005
[47] Krivenkov V, Goncharov S, Nabiev I and Rakovich Y P 2019 Induced transparency in plasmon–exciton nanostructures for sensing applications *Laser Photon. Rev.* **13** 1800176
[48] Zheng P, Semancik S and Barman I 2023 Quantum plexcitonic sensing *Nano Lett.* **23** 9529–37